NONLOCAL EFFECTS ON LOCALIZATION IN A VOID-SHEET

V. TVERGAARD
Department of Solid Mechanics, Technical University of Denmark, Building 404,
DK-2800 Lyngby, Denmark

and

A. NEEDLEMAN
Division of Engineering, Brown University, Providence, RI 02912, U.S.A.

Abstract—For a nonlocal damage model it is expected that the characteristic material length relates to the damage mechanism. In the case of ductile fracture the most relevant length scales would be the average void radius or spacing. Cell model computations representing a single row of voids in an infinite solid under plane strain conditions are here used to compare with predictions of a nonlocal version of a porous ductile material model. Both the critical strain for the onset of plastic flow localization and the slope of the stress–strain curve in the post-localization range are compared, and it is found that both of these are affected by the value of the material length in the nonlocal model. Comparison with predictions of the void-sheet cell model are carried out for an inclined row of voids, leading to shear band failure, as well as a row of transversely aligned voids. For shear bands the material characteristic length scales with the void radius, whereas for transversely aligned voids the scaling is with the void spacing. © 1997 Elsevier Science Ltd.

1. INTRODUCTION

Ductile fracture in structural metals takes place by the nucleation, growth and coalescence of microvoids (Puttick, 1995; Rogers, 1960; Beachem, 1963; Gurland and Plateau, 1963). The voids mainly nucleate at second-phase particles, either by decohesion of the particle-matrix interface or by fracture of the particle, and grow by plastic deformation of the surrounding matrix. In some cases, coalescence simply involves necking down of the ligament between neighboring voids. However, engineering alloys often contain two size scales of void nucleating particles; for example, in steels sulfide inclusions of the order of 10–100 μm and carbides of the order of 0.1–1.0 μm. Then, growth of voids nucleated from the larger inclusions can precipitate the nucleation and growth of smaller scale voids which focus the deformation in a relatively narrow band (Cox and Low, 1974; Latridou and Pineau, 1981). The formation of such a void sheet acts to accelerate the process of coalescence.

A phenomenological constitutive relation for a progressively cavitating solid was introduced by Gurson (1977) and modified by Tvergaard (1981, 1982) and Tvergaard and Needleman (1984). Analyses carried out within the framework of this modified Gurson model have reproduced observed ductile fracture behavior in remarkable detail (Tvergaard and Needleman, 1984; Needleman and Tvergaard, 1987; Tvergaard and Needleman, 1992). However, the modified Gurson model does not incorporate a material length scale. Hence, unless a length scale is somehow included in the problem formulation, numerical predictions of ductile fracture show an inherent mesh sensitivity. In studies of ductile crack growth where the size and spacing of the larger inclusions is directly specified, this introduces a length scale and removes the inherent mesh dependence (Needleman and Tvergaard, 1994). Such an approach, of course, is only possible when the fracture process involves multiple size scales of voids.

However, in other circumstances there is a need for a phenomenological approach where a material length scale is directly incorporated into the constitutive relation. Nonlocal

constitutive relations where the delocalization is related to the damage mechanism have been proposed by Pijauder-Cabot and Bazant (1987) and Barenblatt (1992). Using such ideas, a nonlocal version of the Gurson constitutive relation has been developed by Leblond *et al.* (1994) and by Sun and Hönig (1994). Tvergaard and Needleman (1995a) have incorporated the nonlocal formulation of Leblond *et al.* (1994) into an elastic–viscoplastic version of the Gurson constitutive relation for a progressively cavitating solid (Pan *et al.*, 1983) and have investigated the effect of the material characteristic length in predictions of flow localization into a shear band, failure in metal–matrix composites and void sheet development (Tvergaard and Needleman, 1995a,b).

In these nonlocal formulations, the material characteristic length is introduced as an additional phenomenological parameter in the modified Gurson model. The parameters that enter the local form of the modified Gurson model are either directly measurable material properties, e.g. the volume fraction of void nucleating particles, or have values that are set by comparisons with micromechanical analyses of the growth and coalescence of discrete voids (Tvergaard, 1981, 1982; Tvergaard and Needleman, 1984; Koplik and Needleman, 1988; Tvergaard, 1990). Discrete void studies of coalescence with two size scales of voids have recently been carried out by Faleskog and Shih (1995) and Tvergaard (1996). What has been lacking in the nonlocal theory is a micromechanical basis for assigning the material characteristic length.

In the present paper, we carry out calculations of localization in a void sheet using two approaches. In one case, the voids are modelled discretely as in Tvergaard (1989). In the other case, the nonlocal formulation in Tvergaard and Needleman (1995a) is used. Comparisons of the results of the two calculations are used to identify the material characteristic length entering the nonlocal formulation.

2. PROBLEM DESCRIPTION

In numerical studies of plastic flow localization, based on the Gurson model with a material length scale incorporated, it has been found that the predicted width of shear bands is controlled by the incorporated length scale (Leblond *et al.*, 1994; Tvergaard and Needleman, 1995a). The length scales of importance in a porous ductile material are the void spacing and the void diameter, but so far no investigation has specified how these lengths should affect the choice of a material length in the nonlocal model. Here, numerical studies of localization in a void-sheet, with the voids discretely represented (Tvergaard, 1989), will be used to estimate the relevant material length to be incorporated in the nonlocal model.

2.1. Nonlocal Gurson model

The type of nonlocal evolution equation for the void volume fraction proposed by Leblond *et al.* (1994) was implemented in an elastic–viscoplastic model for a ductile porous material by Tvergaard and Needleman (1995a). This material model, accounting for large deformations, is here described in terms of a convected coordinate, Lagrangian formulation of the field equations, where g_{ij} and G_{ij} are metric tensors in the reference configuration and the current configuration, respectively, with determinants g and G and $\eta_{ij} = 1/2(G_{ij}\text{-}g_{ij})$ is the Lagrangian strain tensor. The contravariant components τ^{ij} of the Kirchhoff stress tensor and σ^{ij} of the Cauchy stress tensor on the current base vectors are related by the expression $\tau^{ij} = \sqrt{G/g}\,\sigma^{ij}$.

In Gurson's (1977) constitutive relations the yield conditions are of the form $\Phi(\sigma^{ij}, \sigma_M, f) = 0$, where σ^{ij} denotes the average macroscopic Cauchy stress tensor, σ_M is an equivalent tensile flow stress representing the actual microscopic stress state in the matrix material and f is the current void volume fraction. The flow potential to be used in the elastic-viscoplastic formulation is of the form

$$\Phi = \frac{\sigma_e^2}{\sigma_M^2} + 2q_1 f^* \cos h\left[\frac{q_2 \sigma_k^k}{2\sigma_M}\right] - 1 - q_1^2 f^{*2} = 0 \tag{1}$$

where the macroscopic effective Mises stress is $\sigma_e = (3s_{ij}s^{ij}/2)^{1/2}$, with $s^{ij} = \sigma^{ij} - G^{ij}\sigma_k^k/3$. The parameters q_1 and q_2 were introduced by Tvergaard (1981, 1982) to bring predictions of the model into closer agreement with full numerical analyses of periodic arrays of voids. The function $f^*(f)$ accounts for the effects of rapid void coalescence at failure and is taken to have the form (Tvergaard and Needleman 1984),

$$f^* = \begin{cases} f & f \leqslant f_c \\ f_c + \dfrac{f_u^* - f_c}{f_f - f_c}(f - f_c) & f \geqslant f_c \end{cases} \tag{2}$$

The onset of rapid void coalescence is assumed to begin at a critical void volume fraction, f_c, with $f_u^* = 1/q_1$. Then, as $f \to f_f$, the material loses all stress carrying capacity ($f^* \to f_u^*$).

Some computations in the present paper are carried out using $f^*(f) \equiv f$, in order to separate effects of porosity induced localization from those of failure. The parameter values are taken to be $q_1 = 1.5$ and $q_2 = 1$ and, when (2) is used, $f_f = 0.25$ for various values of f_c. No void nucleation is accounted for in the present investigation, so here the rate of increase of the local void volume fraction is entirely due to the growth of existing voids

$$\dot{f}_{local} = (1 - f)G^{ij}\dot{\eta}_{ij}^P. \tag{3}$$

The rate of increase of the void volume fraction in the material point at location x^i in the reference configuration is obtained from the local values in (3) by (Leblond et al., 1994; Pijauder-Cabot and Bazant, 1987)

$$\dot{f}(x^i) = \frac{1}{W(x^i)} \int_V \dot{f}_{local}(\hat{x}^i)w(x^i - \hat{x}^i)\,\mathrm{d}\hat{V} \tag{4}$$

where V is the volume of the body in the reference configuration and we use

$$w(z^i) = \left[\frac{1}{1 + \left(\dfrac{z}{L}\right)^p}\right]^q, \quad W(x^i) = \int_V w(x^i - \hat{x}^i)\,\mathrm{d}\hat{V} \tag{5}$$

with $z = (z_iz^i)^{1/2}$ and $p = 8$, $q = 2$, for a material characteristic length $L > 0$. The local formulation corresponds to the limit $L \to 0$. With $L > 0$, $\dot{f}(x^i) \equiv \dot{f}_{local}$ when $\dot{f}_{local}$ is spatially uniform. Hence, nonlocality is associated with spatial gradients in $\dot{f}$. As seen in Fig. 1, the
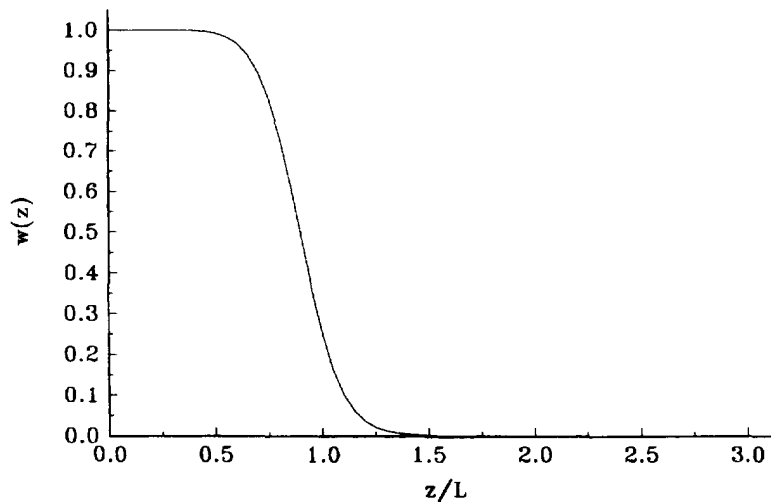

Fig. 1. Delocalization function (5) with $p = 8$ and $q = 2$.

function w is such that $w > 0$ for $z < L$ and $w \approx 0$ for $z > L$, with a relatively narrow transition region. In the computations a cutoff length, $L_c = 1.5L$, is specified such that w in (5) is taken to be zero for $z > L_c$.

The matrix material is assumed to be an elastic–viscoplastic solid as in Pan et al. (1983) and the plastic part of the strain-rate is obtained from the flow potential as

$$\dot{\eta}_{ij}^P = \left[\frac{(1-f)\sigma_M \dot{\varepsilon}_M^P}{\sigma^{k\prime} \dfrac{\partial \Phi}{\partial \sigma^{k\prime}}} \right] \frac{\partial \Phi}{\partial \sigma^{ij}}$$ (6)

with the matrix plastic strain rate, $\dot{\varepsilon}_M^P$, given by

$$\dot{\varepsilon}_M^P = \dot{\varepsilon}_0 \left[\frac{\sigma_M}{g(\varepsilon_M^P)} \right]^{1/m}, \quad g(\varepsilon_M^P) = \sigma_0 [1 + \varepsilon_M^P / \varepsilon_0]^N$$ (7)

where $\varepsilon_M^P = \int \dot{\varepsilon}_M^P \, dt$.

The total strain-rate is taken to be the sum of an elastic part and a plastic part, $\dot{\eta}_{ij} = \dot{\eta}_{ij}^E + \dot{\eta}_{ij}^P$, so that with the elastic stress strain relationship $\overset{\triangledown}{\sigma}{}^{ij} = \mathscr{R}^{ijk\prime}\dot{\eta}_{k\prime}^E$, the elastic–viscoplastic constitutive law takes the form

$$\overset{\triangledown}{\sigma}{}^{ij} = \mathscr{R}^{ijk\prime}\dot{\eta}_{k\prime} - \left[\frac{(1-f)\sigma_M \dot{\varepsilon}_M^P}{\sigma^{mn} \dfrac{\partial \Phi}{\partial \sigma^{mn}}} \right] \mathscr{R}^{ijk\prime} \frac{\partial \Phi}{\partial \sigma^{k\prime}}.$$ (8)

The numerical analyses for a nonlocal porous material in the present investigation are carried out for a rectangular region with periodicities leading to symmetry conditions all around. The details of the numerical solution procedure have been given by Tvergaard and Needleman (1995a) and shall not be repeated here. This also includes the way in which the precalculated influence matrix, corresponding to (4), accounts for values of $\dot{f}_{local}$ outside the region analysed, determined by symmetries. It is noted that in applying the rate tangent formulation of Pierce et al. (1984) the tangent modulus computation is complicated by the nonlocal nature of the constitutive relation. The basis for the computation of a tangent modulus is the consistency relation

$$\frac{\partial \Phi}{\partial \sigma^{ij}} \overset{\triangledown}{\sigma}{}^{ij} + \frac{\partial \Phi}{\partial \sigma_M} \dot{\sigma}_M + \frac{\partial \Phi}{\partial f} \dot{f} = 0$$ (9)

where $\dot{f}$ is given by (4). In the calculations the approximation is made that $\dot{f}$ is replaced by $K\dot{f}_{local}$, with $K = \dot{f}/\dot{f}_{local}$ from the previous time step (or $K = 1$ for $\dot{f}_{local} < 10^{-10}$).

2.2. Void-sheet cell model

A row of uniformly spaced circular cylindrical holes with initial radius R_0 and spacing $2D_0$ is considered, as illustrated in Fig. 2. The principal macroscopic true stresses are σ_1 and σ_2 in the x^1- and x^2-directions, respectively, where the initial angle of inclination between the row of holes and the x^1-axis is ψ_0. The block of material is assumed sufficiently large relative to the void spacing, so that the material far from the void-sheet behaves as a uniformly strained material subject to the prescribed stress history. The distance between the two dashed lines parallel with the void-sheet in Fig. 2 is chosen large enough, so that these lines are in the uniformly strained material region (Tvergaard, 1989).

The band is divided into a number of cells with sides parallel to the x^2-axis. The initial width of a cell is $2A_0 = 2D_0 \cos \psi_0$ and the initial height is B_0, so that the initial width of the band analysed is $2B_0 \cos \psi_0$. Since the solution is periodic along the void sheet, with a
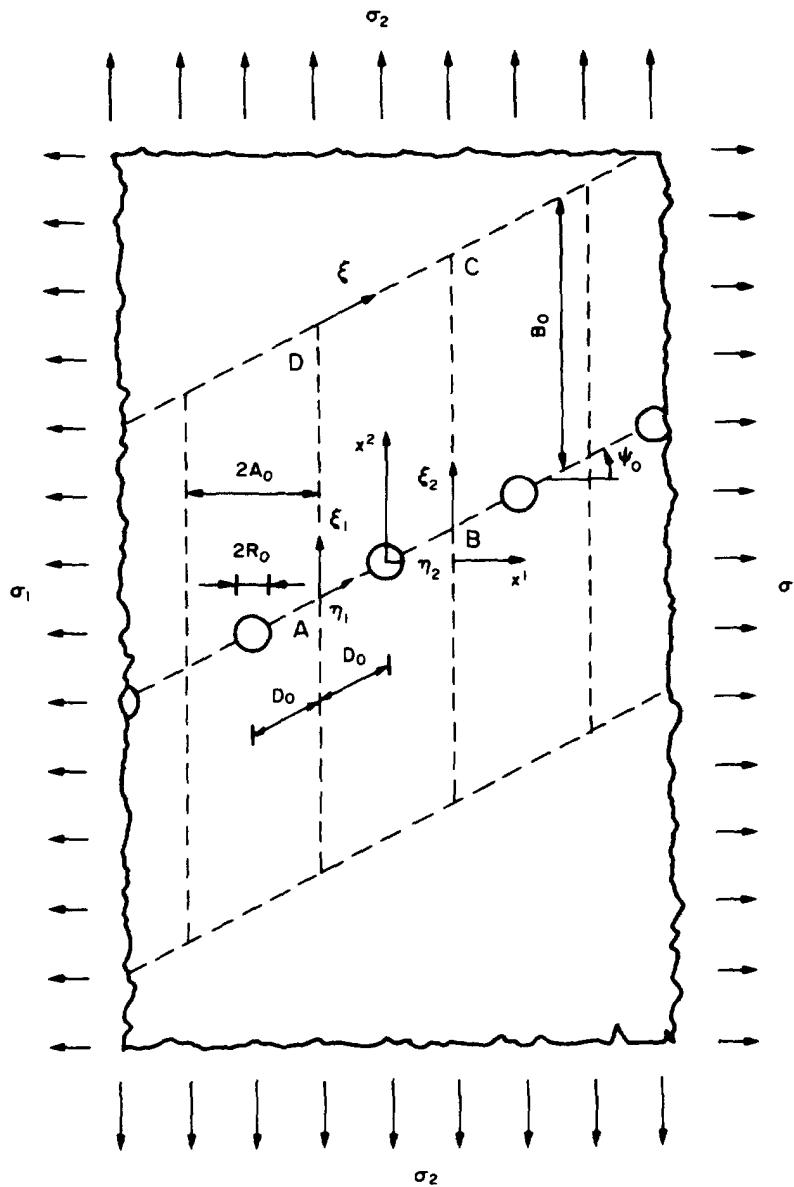
Fig. 2. Material containing a row of uniformly spaced circular cylindrical voids. The region ABCD
is analysed numerically.

period corresponding to the void spacing, all the cells undergo identical behavior. Therefore,
in the numerical solution it is only necessary to analyse one of the cells, i.e. the region
ABCD shown in Fig. 2. The analyses are carried out for conditions of plane strain.

When the current principal logarithmic strain in the field outside the band are ε_1^0 and
ε_2^0 (in the x^1- and x^2-directions, respectively), the current angle of inclination ψ of the void
sheet is given by

$$\tan\psi = e^{(\varepsilon_2^0 - \varepsilon_1^0)}\tan\psi_0. \tag{10}$$

The boundary conditions are specified in terms of the Cartesian displacement components
u^i and the nominal traction components T^i. When it is assumed that the center of the void
belonging to the cell ABCD does not move, the displacement components u_A^i and u_B^i at the
two corner points A and B are determined by the strains ε_1^0 and ε_2^0 outside the band, and
the rotation (10) as

$$u_B^1 = -u_A^1 = A_0(e^{e_1^0} - 1)$$ (11)

$$u_B^2 = -u_A^2 = A_0(e^{e_1^0} \tan\psi - \tan\psi_0).$$ (12)

Similar conditions apply to the edge DC, but here the displacements are also assumed to vary linearly between the two corners, to give complete compatibility with the far field. Thus, in terms of the length measuring coordinate ξ on DC the displacements are

$$u^1(\xi) = u_D^1 + \frac{\xi}{2D_0}(u_B^1 - u_A^1), \quad u^2(\xi) = u_D^2 + \frac{\xi}{2D_0}(u_B^2 - u_A^2).$$ (13)

Furthermore, the resultant forces on the edge DC must agree with the stress field outside the band

$$\int_0^{2D_0} T^2 \, d\xi = \sigma_2(2A_0 + u_B^1 - u_A^1)$$ (14)

$$\int_0^{2D_0} T^1 \, d\xi = -\sigma_1(2D_0 \sin\psi_0 + u_B^2 - u_A^2).$$ (15)

On the cell sides AD, BC and AB the periodicity and symmetry conditions are such that equilibrium and compatibility with the neighbouring cells is satisfied. This is expressed by using the length measuring coordinates ξ_1, ξ_2, η_1 and η_2 (see Fig. 2). Thus, for $\xi_1 = \xi_2$ or $\eta_1 = \eta_2$, respectively,

$$u^1(\xi_1) - u_A^1 = u^1(\xi_2) - u_B^1, \quad u^2(\xi_1) - u_A^2 = u^2(\xi_2) - u_B^2$$ (16)

$$T^1(\xi_1) = -T^1(\xi_2), \quad T^2(\xi_1) = -T^2(\xi_2)$$ (17)

$$u^1(\eta_1) = -u^1(\eta_2), \quad u^2(\eta_1) = -u^2(\eta_2)$$ (18)

$$T^1(\eta_1) = T^1(\eta_2), \quad T^2(\eta_1) = T^2(\eta_2).$$ (19)

The conditions at the void surface, $(x^1)^2 + (x^2)^2 = R_0^2$, are

$$T^1 = T^2 = 0.$$ (20)

The ductile material behavior inside the cell is represented by time-independent J_2-flow theory, using the finite strain generalization discussed by Hutchinson (1973). The material is taken to be strain hardening, with the uniaxial stress–strain behavior represented by the power law

$$\varepsilon = \begin{cases} \sigma/E, & \text{for } \sigma \leq \sigma_y \\ (\sigma_y/E)(\sigma/\sigma_y)^{1/N}, & \text{for } \sigma > \sigma_y \end{cases}$$ (21)

where σ_y is the uniaxial stress and n is the strain hardening exponent.

The analysis of this void-sheet cell model is carried out by a finite element solution as has been described in more detail by Tvergaard (1989). The solution outside the band is taken to satisfy the relation

$$\sigma_1^0 = \varrho\sigma_2^0 \tag{22}$$

where ϱ is a fixed ratio between the principal true stresses. The corresponding principal logarithmic strains ε_1^0 and ε_2^0, appearing in (10), (11) and (12), are determined by a simple incremental solution for a homogeneous material subject to (22), so that the variation of the quantities σ_1^0, ε_1^0 and ε_2^0, as functions of the major principal stress σ_2^0, is known *a priori*.

For the cell model the average logarithmic strain ε_2 in the x^2-direction is somewhat larger than ε_2^0, as the deformations in the shear band along the void-sheet grow much larger than those in the uniformly strained region outside. This average logarithmic strain is given by

$$\varepsilon_2 = \ln\left[1 + (u_D^2 - u_A^2)/B_0\right] \tag{23}$$

and the corresponding true stress in the x^2-direction is $\sigma_2 = \sigma_2^0$.

2.3. Comparison of the two models

In order to represent a row of uniformly spaced voids in terms of a porous ductile material model it would be reasonable to assume a narrow band of initial porosity, with no porosity outside. The value of the initial void volume fraction f_1 to be chosen inside the band is not given *a priori*, as a single row of voids is not associated with a well defined material volume. However, if the value of the bandwidth, $2w_0$, is chosen, the value of a uniform void volume fraction inside this band is directly given by the required volume of voids per unit length of the band. Thus, for a constant value of f_1 inside the band the requirement is

$$f_1 \cdot 2w_0 2D_0 = \pi R_0^2 \tag{24}$$

using the initial void spacing $2D_0$ and radius R_0 in Fig. 2. In fact, in the present investigation a sinusoidal variation of f across the band has been chosen, with twice the band width, $4w_0$, such that the volume of voids per unit length of the band is unchanged, relative to the band with uniform fraction in (24) and the peak value, f_1, is still given by (24). The peak value of the void volume fraction in the band is important, as this determines the onset of localization for a local material model ($L = 0$), but the smooth variation of f across the band has the advantage that the mesh need not exactly resolve the band width $2w_0$. For a band with initial angle of inclination ψ_0 relative to the x^1-axis, as in Fig. 2, the distribution of the initial void volume fraction is taken to be specified by

$$f(x^1, x^2) = f_1\left[1 - \cos\frac{\pi(x^2 - x_C^2)}{2w_\psi}\right], \quad \text{for} \quad -2w_\psi \leqslant x^2 - x_C^2 \leqslant 2w_\psi$$

$$x_C^2 = x^1 \tan\psi_0, \quad w_\psi = w_0/\cos\psi_0. \tag{25}$$

The development of a shear band can be studied by analysing a rectangular region with the band along a diagonal, as has been done by Tvergaard and Needleman (1995). The initial height and width of the region analysed are denoted H_0 and C_0, respectively, and these values are chosen such that $\tan\psi_0 = H_0/C_0$, as indicated in Fig. 3(a). Symmetry boundary conditions are assumed in the computations

$$\dot{u}^1 = 0, \quad \dot{T}^2 = 0, \quad \text{at} \quad x^1 = 0 \tag{26}$$

$$\dot{u}^2 = 0, \quad \dot{T}^1 = 0, \quad \text{at} \quad x^2 = 0 \tag{27}$$

$$\dot{u}^1 = \dot{U}_1, \quad \dot{T}^2 = 0, \quad \text{at} \quad x^1 = C_0 \tag{28}$$
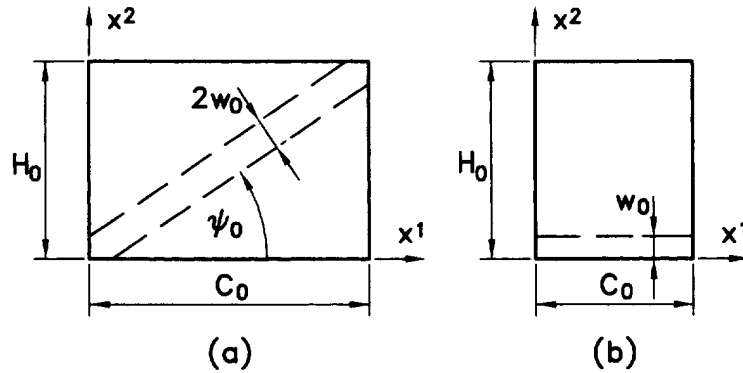
Fig. 3. Rectangular region analysed with nonlocal material model: (a) inclined imperfection band along diagonal; (b) imperfection band representing transversely aligned voids.

$$\dot{u}^2 = \dot{U}_{\mathrm{II}}, \quad \dot{T}^1 = 0, \quad \text{at} \quad x^2 = H_0 \tag{29}$$

where the two constants U_{I} and U_{II} are displacements of the edges and the ratio $\dot{U}_{\mathrm{I}}/\dot{U}_{\mathrm{II}}$ is determined in each increment so that the average principal true stresses have a fixed ratio $\varrho = \sigma_1/\sigma_2$, analogous to that specified by (22). Because of the doubly periodic symmetry, the full configuration corresponding to Fig. 3(a) involves a collection of intersecting shear bands. However, only the shear band contained in the unit cell (Fig. 3(a)) is relevant to the comparison with the unit cell of Fig. 2, for the appropriate choice of the ratio w_0/H_0. The values of the average principal logarithmic strains for the material are $\varepsilon_1 = \ln(1 + U_{\mathrm{I}}/C_0)$ and $\varepsilon_2 = \ln(1 - U_{\mathrm{II}}/H_0)$. Since the region analysed contains the full shear band width, and comparison is made with the average strain (23) for the void-sheet cell mode, the appropriate choice of the height of the region analysed is $H_0 = 2B_0$. As in the analyses of Tvergaard and Needleman (1995a) an equal number of quadrilateral elements is used in the x^1- and x^2-directions, each built up of four triangular elements, so that mesh alignment fascilitates shear band formation along the diagonal.

The void-sheet cell model in Fig. 2 can also be used to analyse flow localization and subsequent void coalescence in a row of transversely aligned voids, i.e. for $\psi_0 = 0°$. Here, comparison with the nonlocal model can be carried out by analysing the region shown in Fig. 3(b), where the band containing the initial imperfection (25) is along the x^1-axis. In this case the region analysed contains only half the width of the imperfection band and therefore the height $H_0 = B_0$ is appropriate for comparison with the cell model in Fig. 2.

A difference between the boundary conditions applied in the two model problems, Fig. 2 and Fig. 3, is that in Fig. 2 the fixed stress ratio (22) is prescribed for the deformation fields outside the band, whereas in Fig. 3 the fixed stress ratio is prescribed for the whole region, including the shear band. This difference will be small as long as the shear band width is small compared to H_0.

Another difference between the two model problems considered here is that the void-sheet unit cell model (Tvergaard, 1989) is formulated for time-independent plasticity, whereas the nonlocal model of Tvergaard and Needleman (1995a) for damage in porous plastic solids is an elastic–viscoplastic material model. Here, the value of the strain-rate hardening exponent in (7) is chose very small, m = 0.00333, so that the predictions of the elastic-viscoplastic model are practically indistinguishable from those of the corresponding time-independent material model. Thus, the value of σ_0/E in (7) is chosen identical to σ_y/E in (21). It is also noted that the power law descriptions (7b) and (21) for strain hardening are not identical, but the difference is negligible in the range considered here.

3. RESULTS

The comparisons to be considered here focus primarily on predictions of localization in inclined shear bands, as has been the main purpose of developing the void-sheet cell model illustrated in Fig. 2. Also the values of the material parameters and the values of
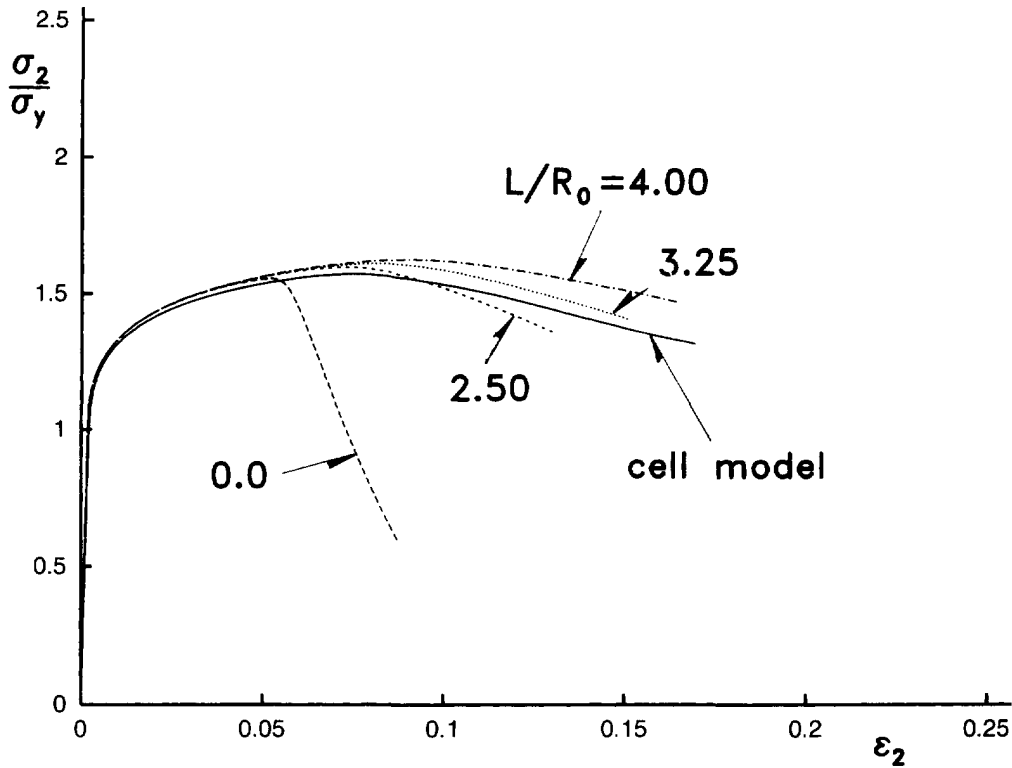
Fig. 4. Stress–strain curve for void-sheet cell model compared with predictions of the nonlocal material model, for $R_0/D_0 = 0.175$, $B_0/A_0 = 4$, $\psi_0 = 30^\circ$, $p = 0$, $f_1 = 0.060$ and different values of L/R_0.

R_0/D_0 are chosen identical to those considered by Tvergaard (1989). Therefore, it is already known that for the range of parameters studied the most critical initial angle of inclination of the row of voids is $\psi_0 \simeq 30^\circ$. In all cases considered the initial yield strain is specified by $\sigma_y/E = 0.002$, Poisson's ratio is $v = 0.3$ and the strain hardening exponent is $N = 0.1$.

In Fig. 4 the solid curve predictions obtained by the void-sheet cell model for $R_0/D_0 = 0.175$, $B_0/A_0 = 4$, $\psi_0 \simeq 30^\circ$ and $\sigma_1/\sigma_2 = 0$. The four dashed, dotted or dash-dotted curves in Fig. 4 show results obtained by the nonlocal version of the elastic-viscoplastic Gurson model, based on analyses for a rectangular region as shown in Fig. 3(a). The peak value of the initial void volume fraction in the inclined band containing the initial imperfection is chosen as $f_1 = 0.060$. Then, using (24) together with the values of R_0/D_0 and B_0/A_0 chosen for the cell model, it is found that the imperfection bandwidth should be specified as $w_0 = 2.291R_0 = 0.1157B_0$. Furthermore, $H_0 = 2B_0$, as discussed above in relation to Fig. 3(a) and a uniform mesh is used for the nonlocal analyses with 40×40 quadrilateral elements. In these analyses for localization in an inclined void-sheet the representation of final failure by void coalescence has been kept inactive by assuming $f^*(f) \equiv f$. This is reasonable, since the onset of localization occurs at a value of f around $1.5f_1$ and since values of f as high as 0.15 are only found near the ends of the post-localization curves shown in Fig. 4. The logarithmic strain ε_2 on one axis in Fig. 4 is the overall strain for the rectangular region in Fig. 3, compared with the strain (23) for the void-sheet cell model, so that in both cases the strain is measured over a length containing the localized shear band as well as a great deal of the uniformly strained region outside.

The void-sheet cell model analysis in Fig. 4 predicts the onset of plastic flow localization (i.e. elastic unloading in the region outside the localized shear band) at $\varepsilon_2 = 0.075$ and the remaining part of the solid curve shows the slope of the post-localization stress–strain curve, which is of course strongly dependent on the length of the region analysed compared to the width of the localized shear band. Predictions of the nonlocal model are shown for four values of L/R_0, i.e. 0.0, 2.50, 3.25 and 4.00. For these four values of the material length L the predicted values of ε_2 at the onset of localization are about 0.054, 0.076, 0.083 and

$\dfrac{\sigma_2}{\sigma_y}$

2.5

2

1.5

1

0.5

0

L/R$_0$ =4.00

2.50

3.25

0.0

cell model

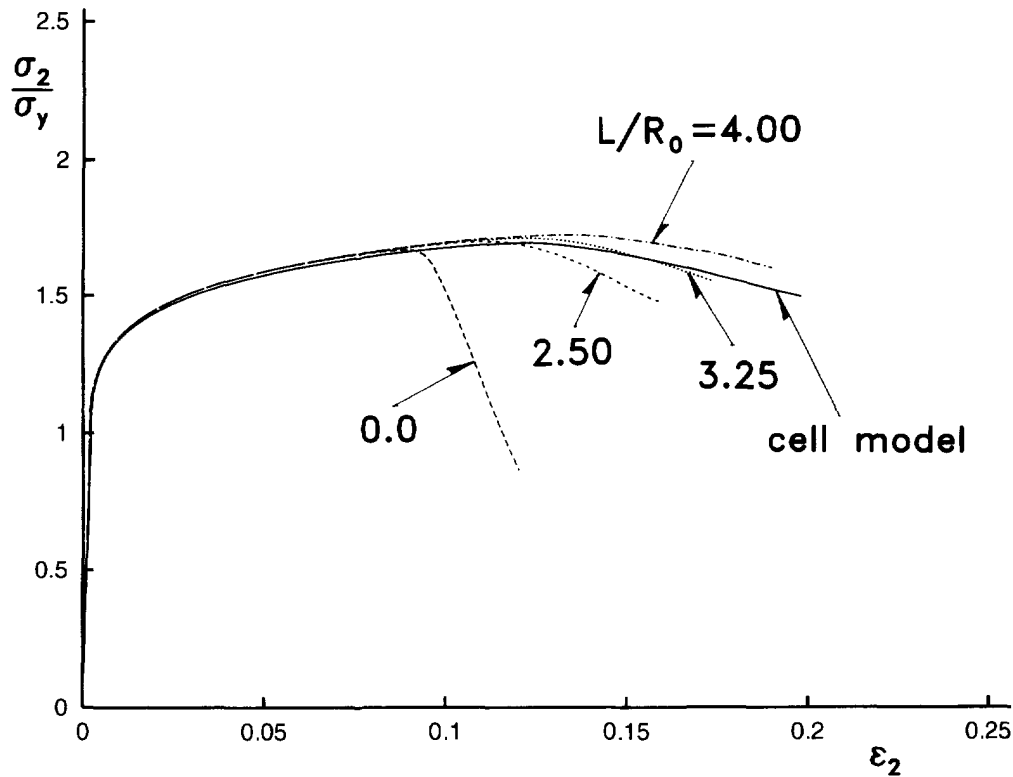0   0.05   0.1   0.15   0.2   0.25

ε_2

Fig. 5. Stress–strain curve for void-sheet cell model compared with predictions of the nonlocal material model, for $R_0/D_0 = 0.125$, $B_0/A_0 = 4$, $\psi_0 = 30^\circ$, $\rho = 0$, $f_1 = 0.040$ and different values of L/R_0.

0.091, respectively. It is seen that the post-localization slopes predicted for the values 2.50, 3.25 and 4.00 of L/R_0 are in reasonably good agreement with the void-sheet cell model, with the better representation obtained for the two larger values. In the limit of the local Gurson model, $L = 0$, the post-localization slope in Fig. 4 gives a poor representation of the cell model and furthermore this prediction is strongly mesh sensitive, as the shear band will be as narrow as allowed for by the mesh. The choice of a material length L larger than the mesh size controls the shear band width and removes the mesh sensitivity (Leblond *et al.*, 1994; Tvergaard and Needleman, 1995a) and it is clear from Fig. 4 that the nonlocal model is able to give a reasonable representation of the post-localization stress–strain relationship. In addition, it is also seen that using this delocalization in the Gurson model results in a delay of the onset of localization. It is noted that in Fig. 4 the ratio between the length L and the element size is 2.5, 3.3 and 4.0, respectively, for the values of 2.50, 3.25 and 4.00 of L/R_0.

A comparison as that in Fig. 4 has also been carried out for a somewhat lower initial peak value of the void volume fraction, $f_1 = 0.055$, with a corresponding larger value of the imperfection bandwidth w_0, according to (24). For $L = 0$ this gives later localization, as was also shown by Tvergaard (1989), but for the non-zero values of L considered in Fig. 4 the difference appears mainly as slightly higher levels of the curves in the post-localization range. Thus, with a realistic level of L and the imperfection bandwidth determined by (24), the predictions are not very sensitive to moderate variations of f_1.

The void-sheet cell model analyses illustrated in Fig. 5 are identical to those in Fig. 4 apart from the relatively smaller voids specified by $R_0/D_0 = 0.125$. This results in significantly later onset of plastic flow localization, at $\varepsilon_2 = 0.121$, but otherwise the shape of the solid curve in Fig. 5 is rather similar to that in Fig. 4. The nonlocal analyses are here carried out for $f_1 = 0.040$, and thus according to (24) the imperfection bandwidth is specified as $w_0 = 2.454R_0 = 0.0886B_0$. The predictions of the nonlocal model for the four values 0.0, 2.50, 3.25 and 4.00 of L/R_0 show that the best agreement with the slope of the solid curve is obtained for 4.00, while the prediction for 3.25 gives a better overall fit. By interpolation
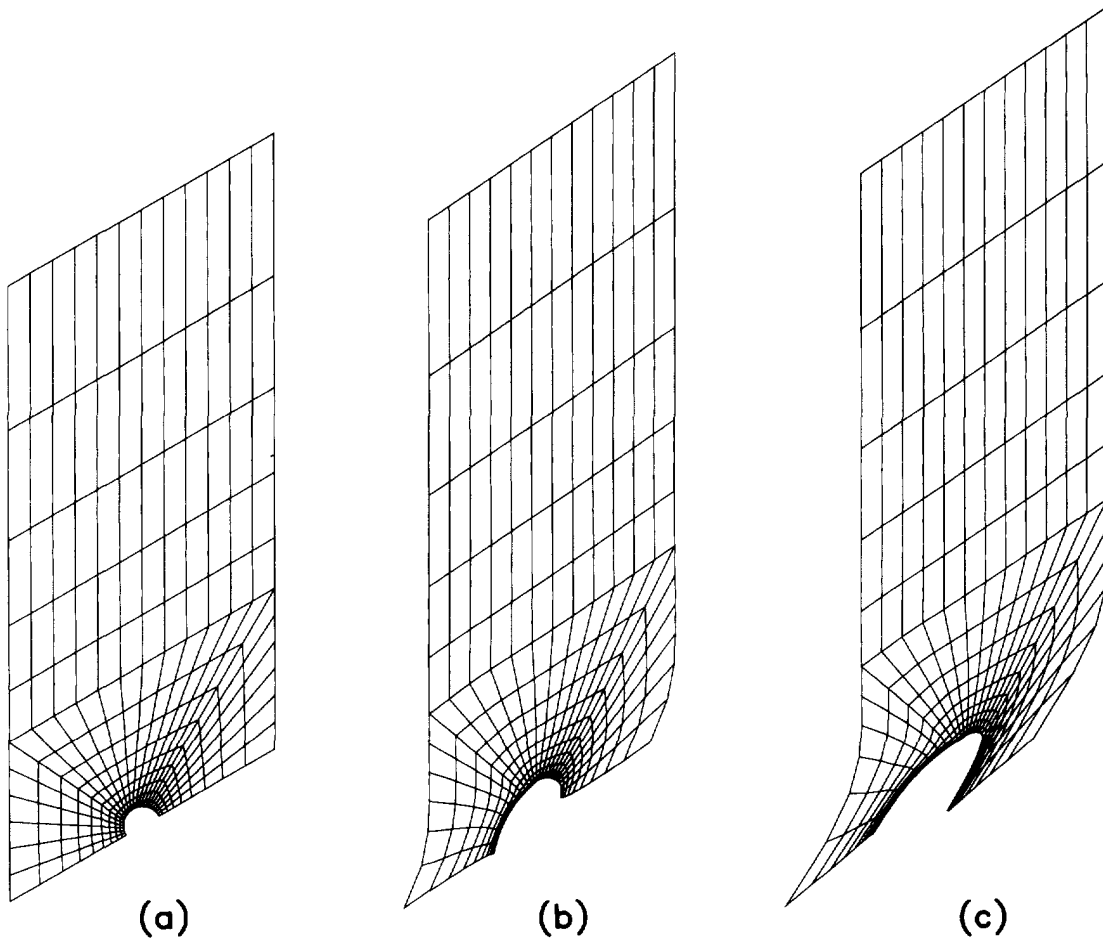
Fig. 6. Initial mesh and two deformed meshes for $R_0/D_0 = 0.125$, $B_0/A_0 = 4$, $\psi_0 = 30°$ and $\rho = 0$: (a) at $\varepsilon_2 = 0$; (b) at $\varepsilon_2 = 0.130$; (c) at $\varepsilon_2 = 0.198$.

between the curves shown in Figs 4 and 5 we may state that optimum choices of L/R_0 in the two figures are about 3.5 and 4.0, respectively, which corresponds to the values 0.61 and 0.50 of L/D_0. Thus, it appears that the appropriate choice of L depends on the void spacing as well as the void radius. The post-localization slope predicted for $L = 0$ is mesh dependent, as mentioned above.

Also the nonlocal computations in Fig. 5 have been repeated with a lower initial peak value of the void volume fraction, $f_1 = 0.035$ and the corresponding larger value of the half imperfection bandwidth w_0. This results in a less good agreement in the post-localization range for appropriately chosen values of L/R_0, as was also found in the analogous comparison relating to Fig. 4; but still it can be concluded that the sensitivity to moderate variations of f_1 is not very strong.

Figure 6 shows the initial mesh and two deformed meshes for the computation giving the solid curve in Fig. 5. A higher number of elements has been used here than that used by Tvergaard (1989) but the result is the same that a shear band somewhat wider than the current void dimension develops. Inside the band, the growing ellipsoidal voids rotate as the localized strains grow large, thus leading to the void pattern characteristic for coalescence in a void-sheet. For the cell model results in Fig. 5 the dependence of the post-localization slope on the mesh has been checked by repeating the computation with 0.44 times as many elements and 1.78 times as many elements, respectively. The comparison shows that the stress does delay a little more rapidly for increasing mesh refinement, but the change is small. In particular, these comparisons show that the lack of a sharp drop off in the cell model curves at the onset of localization is not a result of the mesh chosen. It is noted that
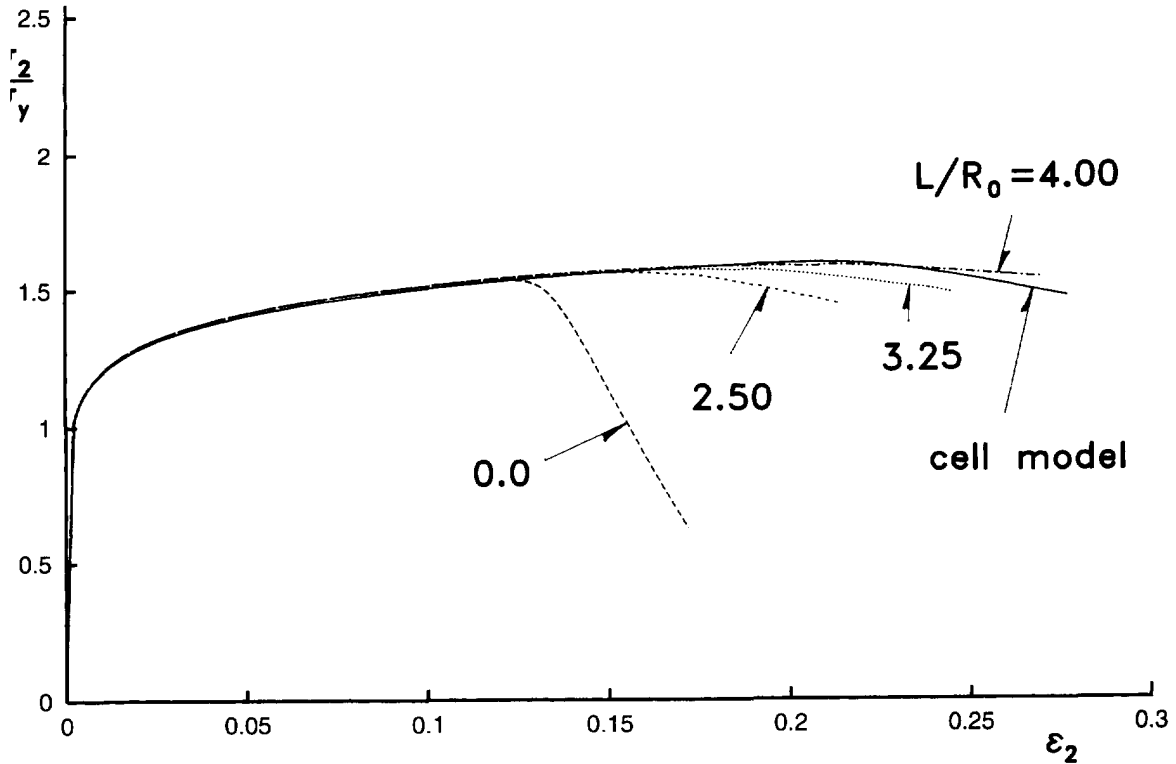
Fig. 7. Stress–strain curve for void-sheet cell model compared with predictions of the nonlocal material model, for $R_0/D_0 = 0.125$, $B_0/A_0 = 4$, $\psi_0 = 30°$, $\rho = 0. - 125$, $f_1 = 0.040$ and different values of L/R_0.

the values of f_1 used in the nonlocal calculations in Figs 4 and 5 give w_0 a little larger than the void diameter.

The effect of the stress state is investigated in Figs 7 and 8, where the values of the fixed ratio, $\varrho = \sigma_1/\sigma_2$, are taken to be -0.125 and 0.125, respectively, while all other parameters are identical to those considered in Fig. 5. Comparison of these three figures shows clearly that the onset of plastic flow localization is delayed for $\varrho < 0$ and hastened for $\varrho > 0$, as was also found by Tvergaard (1989). The point of main interest here is whether or not the same choice of the material length L gives a good representation of the post-localization behavior for different stress states. Although the curves predicted for $L/R_0 = 4.00$ give a useful approximation in all three figures, there clearly is some sensitivity to the stress state. Thus in Fig. 7, for $\varrho = -0.125$, it appears that the optimum choice of material length would be $L/R_0 \simeq 3.25$, whereas in Fig. 8, for $\varrho = 0.125$, a value of L/R_0 somewhat higher than 4.00 would give a better approximation of the post-localization slope.

As has been emphasized above, the slope of the post-localization stress–strain curve depends strongly on the length of the region over which the average strain ε_2 is measured, compared to the width of the shear band. Therefore, the void-sheet cell model computation in Fig. 5, with $R_0/D_0 = 1.25$ and $\varrho = 0$, has been repeated for a larger aspect of ratio of the region analysed, $B_0/A_0 = 6$. In the corresponding nonlocal computations the imperfection band is specified by $f_1 = 0.040$ and $w_0 = 2.454R_0$, as in Fig. 5; but in Fig. 9 the value of the ratio w_0/B_0 is smaller, 0.0590, due to the larger value of B_0/A_0. In order to keep the mesh size unaltered, relative to the imperfection bandwidth, the nonlocal computations are here carried out with 60×60 quadrilateral elements. For the void-sheet cell model, i.e. the solid curve in Fig. 9, the onset of plastic flow localization occurs at $\varepsilon_2 = 0.122$. The negative slope of the stress strain curve in the post-localization range is numerically larger in Fig. 9 than that found in Fig. 5, as would be expected for the higher aspect ratio of the cell model analysed. The most interesting result in Fig. 9 is the fact that the representation obtained by the nonlocal computation for $L/R_0 = 4.00$ is as good as that found in Fig. 5. Thus, it
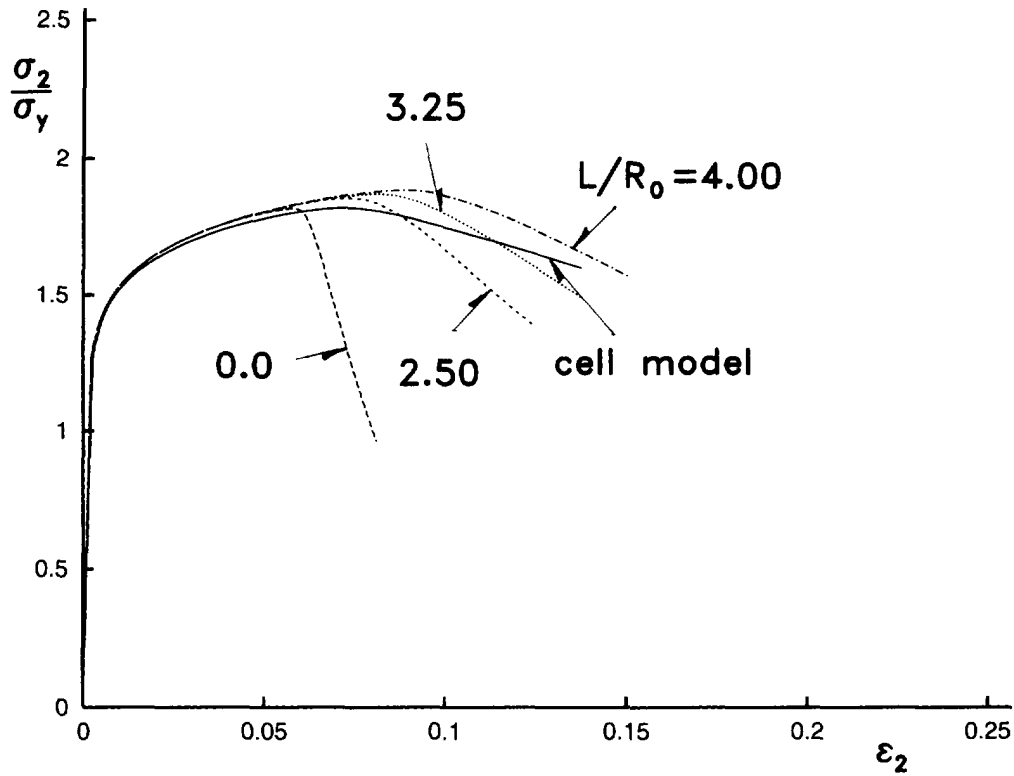
Fig. 8. Stress-strain curve for void-sheet cell model compared with predictions of the nonlocal material model, for $R_0/D_0 = 0.125$, $B_0/A_0 = 4$, $\psi_0 = 30^\circ$, $\rho = 0.125$, $f_1 = 0.040$ and different values of L/R_0.
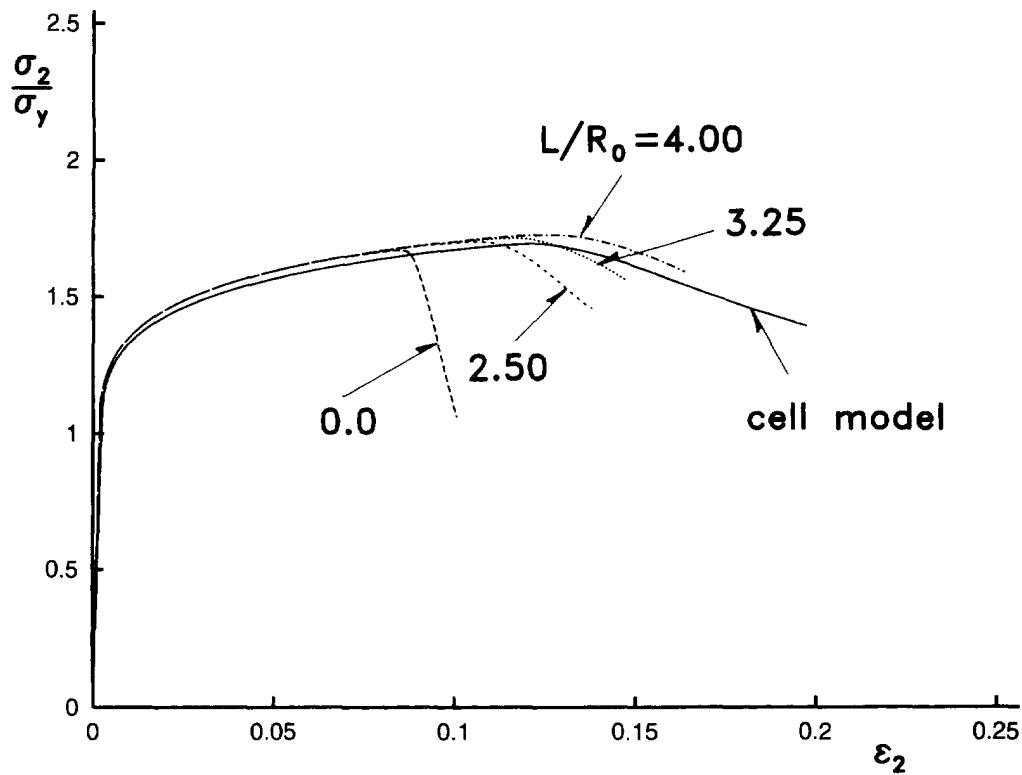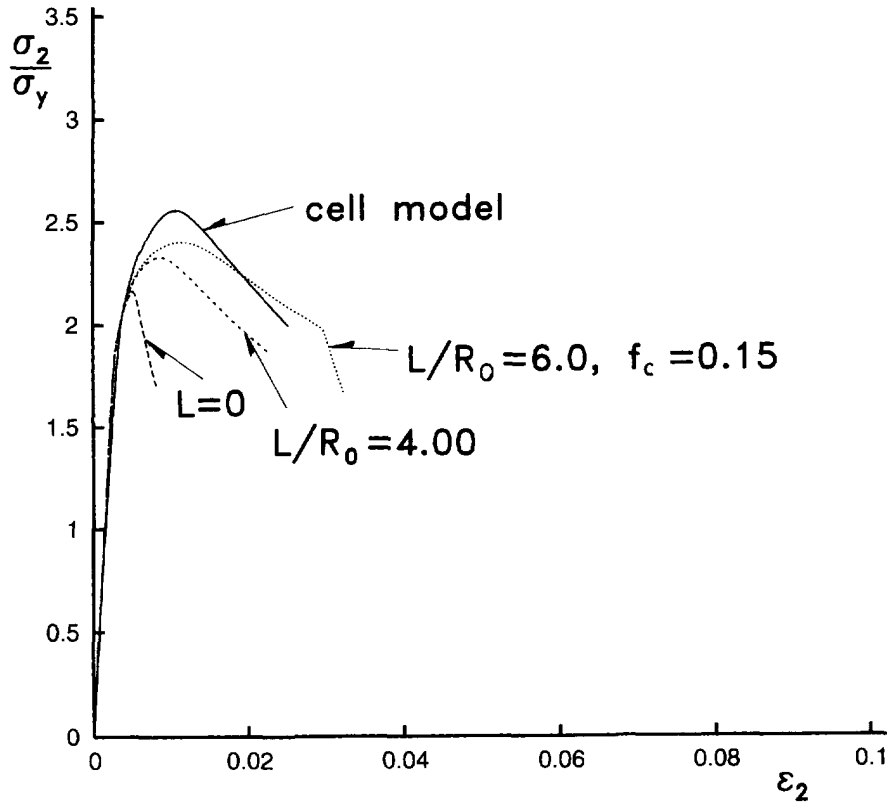

Fig. 9. Stress-strain curve void-sheet cell model compared with predictions of the nonlocal material model, for $R_0/D_0 = 0.125$, $B_0/A_0 = 6$, $\psi_0 = 30^\circ$, $\rho = 0$, $f_1 = 0.040$ and different values of L/R_0.

Fig. 10. Stress–strain curve for void-sheet cell model compared with predictions of the nonlocal material model, for $R_0/D_0 = 0.175$, $B_0/A_0 = 4$, $\psi_0 = 0°$, $\rho = 0.5$, $f_1 = 0.060$ and different values of L/R_0.

appears that a fixed value of the material length, relative to the void dimension or spacing, will give a good representation of plastic flow localization in a void sheet, independent of the specimen size.

As mentioned in Section 2.3 the cell model in Fig. 2 can also be used to analyse flow localization and subsequent void coalescence in a row of transversely aligned voids, i.e. for $\psi_0 = 0°$. This type of analysis is illustrated in Fig. 10, for $R_0/D_0 = 0.175$, $B_0/A_0 = 4.0$ and a fixed stress ratio specified by $\varrho = 0.5$ in (22). The values of the material parameters are identical to those considered in the previous cases. In the nonlocal studies for $\psi_0 = 0°$ only half of the imperfection bandwidth is enclosed in the region analysed (see Fig. 3(b)), so that $H_0 = B_0$. Furthermore, the width of the region analysed is taken to be $C_0 = A_0$ and a uniform 30×30 mesh of quadrilaterals is used. In Fig. 10 the onset of plastic flow localization predicted by the void-sheet cell model is at $\varepsilon_2 = 0.0108$, and subsequent flow is confined to the ligaments between neighbouring voids, leading towards void coalescence.

The predictions of the nonlocal model in Fig. 10 are obtained for $f_1 = 0.060$, as in Fig. 4, with the corresponding imperfection bandwidth $w_0 = 2.291R_0 = 0.100B_0$ according to (24). The values of L/R_0 are 0.0, 4.0 and 6.0, respectively and $f_c = 0.15$ is used in all cases. For $L = 0$ the onset of localization is predicted at too small values of both stress and strain. However, as was also found for the inclined void-sheets, the non-zero values of L result in a significant delay of the onset of localization, which means in the case of Fig. 10 that both the stress and the strain at the onset of localization are increased. For $L/R_0 = 4.0$, which gave a rather good representation in Figs 4–9, the values of stress and strain at the onset of localization are much increased, but not quite large enough. However, the post-localization slope is in rather good agreement with the void-sheet cell model. For $L/R_0 = 6.0$ the localization strain is well represented, while the localization stress is still a bit too low. In the post-localization range this curve is initially not steep enough and subsequently too steep when $f > f_c$ in the band, but generally this curve gives a rather good approximation.
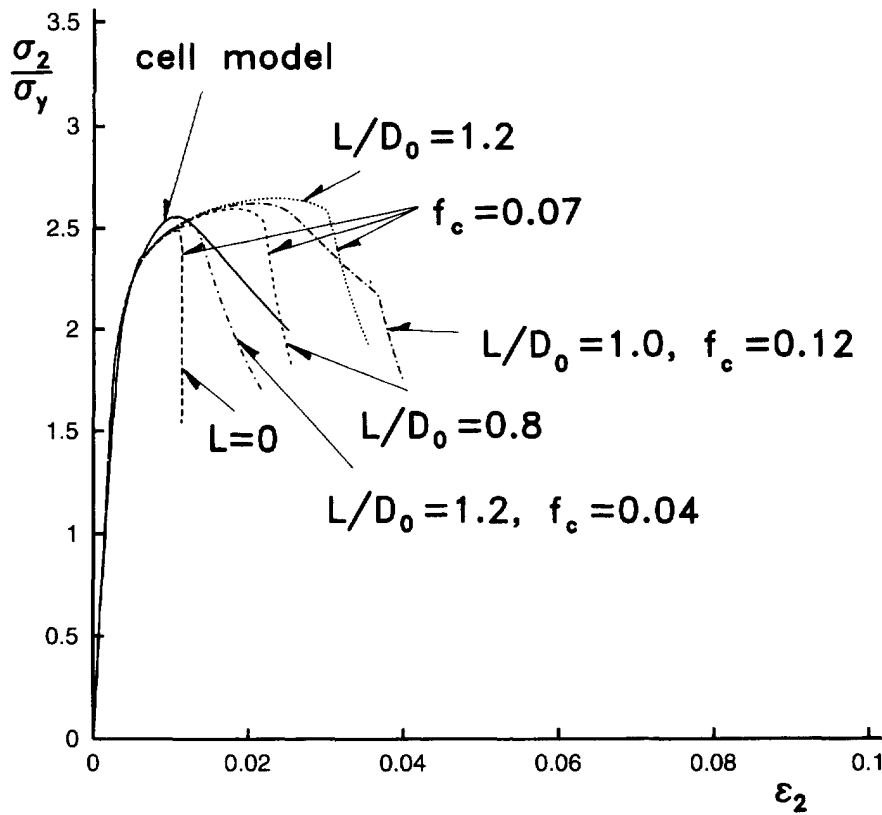
Fig. 11. Stress–strain curve for void-sheet cell model compared with predictions of the nonlocal material model, for $R_0/D_0 = 0.175$, $B_0/A_0 = 4$, $\psi_0 = 0^c$, $\rho = 0.5$, $f_1 = 0.038$ and different values of L/R_0.

Attempts to obtain a better approximation of the peak stress have been carried out by using a smaller initial peak value of the void volume fraction, $f_1 = 0.038$, with the corresponding imperfection bandwidth $w_0 = 3.617R_0 = 0.158B_0$ according to (24). In Fig. 11 the curve for $L/D_0 = 1.0$ (i.e. $L/R_0 = 5.71$) and $f_c = 0.12$ shows that the onset of localization is significantly delayed, while the post-localization slope is well represented as long as $f < f_c$. For $f > f_c$ the coalescence model (2) results in a much steeper post-localization curve. For $L = 0$ the onset of localization occurs at $\varepsilon_2 = 0.011$, in better agreement with the cell model; but the post-localization slope depends on the mesh. The effect of choosing a smaller value of f_c is illustrated in Fig. 11 by three curves for $f_c = 0.07$. These three curves show that the delay in the onset of localization is only slightly affected by the smaller value of f_c, but the post-localization behavior is too steep in all cases, although the slope improves for increasing L. For the larger value of the material length, $L/D_0 = 1.2$, two different curves are shown in Fig. 11, where the curve for $f_c = 0.04$ illustrates that a realistic strain for the onset of localization can be enforced by using a low value of f_c. However, the conclusion of these attempts is that the two curves for non-zero values of L in Fig. 10 give a better approximation than any of the curves in Fig. 11.

Apart from the relatively smaller voids, $R_0/D_0 = 0.125$, the cell model analysis illustrated in Fig. 12 is identical to that of Fig. 10. The main effect of the smaller voids is a later onset of the plastic flow localization, here at $\varepsilon_2 = 0.0245$. Results of nonlocal analyses are shown for $f_1 = 0.040$, as in Figs 5–9, with the corresponding imperfection bandwidth $w_0 = 2.454R_0 = 0.0767B_0$. As in Fig. 10 $L = 0$ results in too low values of the stress and strain at the onset of localization. Using $L/R_0 = 4.0$ gives a noticeable improvement and a rather good representation of the post-localization slope. The result for $L/R_0 = 6.0$ in Fig. 12 is not quite as good as that in Fig. 10, whereas the curve for $L/R_0 = 8.4$ in Fig. 12 is more like that for $L/R_0 = 6.0$ in Fig. 10. It is noted that both these curves correspond to $L/D_0 = 1.05$, with the different values of R_0/D_0 in the two figures. Thus, for a row of voids
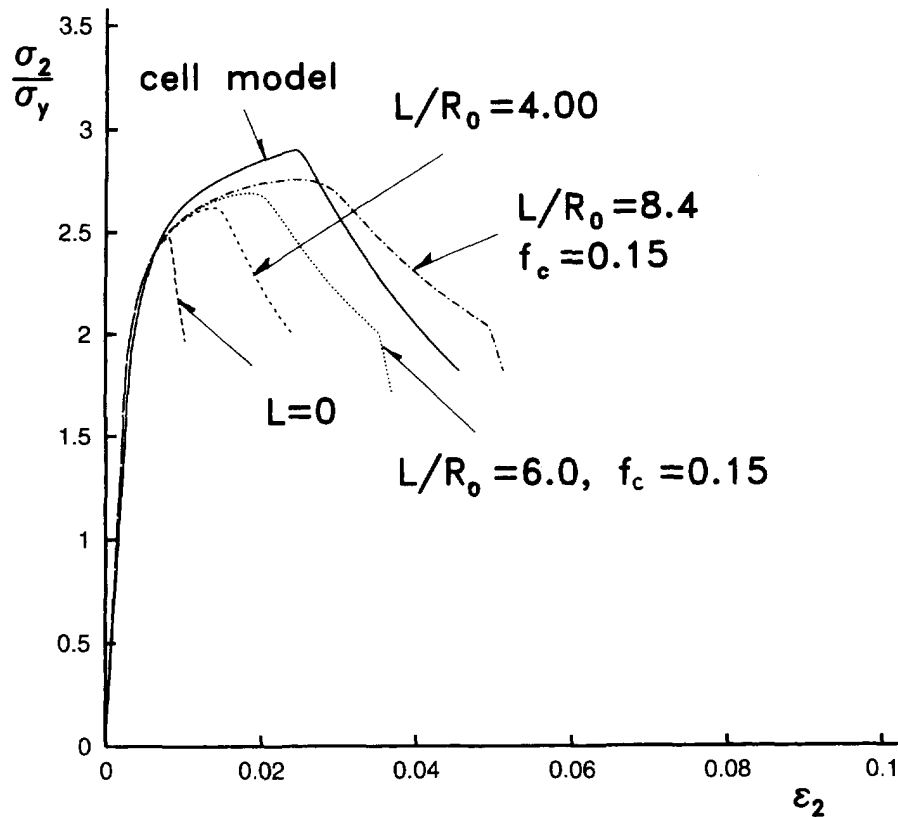
Fig. 12. Stress–strain curve for void-sheet cell model compared with predictions of the nonlocal material model, for $R_0/D_0 = 0.125$, $B_0/A_0 = 4$, $\psi_0 = 0^\circ$, $\rho = 0.5$, $f_1 = 0.040$ and different values of L/R_0.

with $\psi_0 = 0^\circ$ it appears that the appropriate material length L scales with the void spacing rather than the void radius. By contrast, the comparison of Figs 4 and 5 above indicated that for $\psi_0 = 30^\circ$ the best value of L scales better with the void radius than with the void spacing.

4. DISCUSSION

Discrete void cell model studies of localization have been carried out and compared with the predictions of a nonlocal phenomenological constitutive relation for a progressively cavitating solid. These comparisons provide a micro-mechanical basis for specifying the material characteristic length that enters the constitutive relation. Two modes of localization are considered: localization in a void sheet ($\psi_0 \neq 0^\circ$) and localization of a row of transversely aligned voids ($\psi_0 = 0^\circ$). This latter case corresponds to the necking down of the ligaments between voids aligned perpendicular to the maximum principal stress direction. In either case, the onset of localization marks the initiation of coalescence.

For the homogenized local, rate-independent theory the post-localization response is highly mesh dependent (material rate dependence can overcome this, but with a characteristic length that is generally much smaller than the void size or spacing). On the other hand, for the nonlocal continuum, with the characteristic material length specified in terms of an integral condition on the void volume fraction rate, this mesh sensitivity is not present.

In all cases, the results for the early stages of void growth are not very sensitive to the value of the material characteristic length. On the other hand, the onset of localization and the post-localization response depend sensitively on the value of the material characteristic length. Comparison with the discrete cell model results indicates that for localization in a void sheet the material characteristic length scales with the void radius, whereas for necking down of the ligament between voids the scaling is with the void spacing. This latter behavior

is consistent with the results in Koplik and Needleman (1988) where a dependence on void spacing was found for an axisymmetric discrete void cell model with the voids aligned perpendicular to the maximum principal stress direction.

The stress–strain curves calculated here by the nonlocal Gurson model show clearly that the overall strain at the onset of localization increases for increasing value of L/R_0. For bifurcation into a localized mode Pijaudier-Cabot and Benallal (1993) and Leblond et al. (1994), using a delocalization similar to (4), have found that the first critical bifurcation strain for the nonlocal model is identical to that for the local model. The same result was found by Benallal and Tvergaard (1995) in a bifurcation study for strain gradient plasticity. However, in all these cases the first critical bifurcation for the nonlocal solids corresponds to the long wavelength limit, whereas bifurcations into shorter wavelength modes are delayed. The material considered in the present paper is viscoplastic, so that bifurcation is irrelevant, but here all results depend on the initial imperfections, and the sensitivity to L/R_0 is part of the imperfection sensitivity.

For both localization in a void sheet and for necking down of the ligament between voids, the fitting is rather approximate. A single value of the material characteristic length is not always found that provides a very good fit to both the onset of localization and to the post-localization response. The fit is generally better for localization in a void sheet, with L in the range of $3.25–4.0R_0$ providing a reasonably good representation of the discrete void cell model response in Figs 4–5 and 7–9. Comparison of Figs 5, 7 and 8 shows that the best fit value of L is somewhat stress state dependent. However, Fig. 9 shows that the best fit value of L is rather insensitive to the overall specimen dimensions for a fixed void size. In Figs 10–12, where $\psi_0 = 0°$ so that coalescence involves necking down of the ligament between voids, a value of L around D_0 provides a reasonable fit. It is interesting to note that the classic void coalescence model of Brown and Embury (1973) has the void spacing as the characteristic length.

Continuum mechanics analyses of ductile failure have generally been based on a local constitutive description of progressive cavitation. This is a good approximation for the early stages of void growth. However, once localization leading to coalescence takes place, the present results indicate that a characteristic length is needed to provide an accurate phenomenological description of the subsequent response. The approach used here is one where the material characteristic length enters the formulation through an integral condition on the void volume fraction rate. Other nonlocal formulations are possible and it remains to be seen which provides the most accurate description of the post-localization response leading to void coalescence.

REFERENCES

Barenblatt, G. I. (1992). Micromechanics of fracture. Proc. Int. Congr. Theory of Applied Mechanics, Haifa.

Beachem, C. D. (1963). An electron fractographic study of the influence of plastic strain conditions upon ductile rupture processes in metals. Transactions of the ASM 56, 318.

Benallal, A. and Tvergaard, V. (1995). Nonlocal continuum effects on bifurcation in the plane strain tension–compression test. Journal of Mechanics, Physics and Solids 43, 741-770.

Brown, L. M. and Embury, J. D. (1973). The initiation and growth of voids at second phase particles. Proc. 3rd Int. Conf. on Strength of Metals and Alloys, Institute of Metals, London, pp. 164-169.

Cox, T. B. and Low, J. R. (1974). An investigation of the plastic fracture of AISI 4340 and 18 nickel-200 grade maraging steels. Metallurgical Transactions 5, 1457-1470.

Faleskog, J. and Shih, C. Fong (1995). Micromechanics of coalescence—1. Synergetic effects of elasticity, plastic yielding and multi-size-scale voids. Brown University Report.

Gurland, J. and Plateau, J. (1963). The mechanism of ductile rupture of metals containing inclusions. Transactions of the ASM 56, 442.

Gurson, A. L. (1977). Continuum theory of ductile rupture by void nucleation and growth—1. Engineering Material Technology 99, 2-15.

Hutchinson, J. W. (1973). Finite strain analysis of elastic–plastic solids and structures. In Numerical Solution of Nonlinear Structural Problems (Edited by R. F. Hartung), p. 17.

Koplik, J. and Needleman, A. (1988). Void growth and coalescence in porous plastic solids. *International Journal of Solids and Structures* **24**, 835.

Latridou, J. C. and Pineau, A. (1981). Crack initiation and stable crack growth resistance in A508 steels in relation to inclusion distribution. *Engineering Fracture Mechanics* **15**, 55–71.

Leblond, J. B., Perrin, G. and Devaux, J. (1994). Bifurcation effects in ductile metals with damage delocalization. *Journal of Applied Mechanics* **61**, 236–242.

Needleman, A. and Tvergaard, V. (1987). An analysis of ductile rupture modes at a crack tip. *Journal of Mechanics, Physics and Solids* **35**, 151–183.

Needleman, A. and Tvergaard, V. (1994). Mesh effects in the analysis of dynamic ductile crack growth. *Engineering Fracture Mechanics* **47**, 75–91.

Pan, J., Saje, M. and Needleman, A. (1983). Localization of deformation in rate sensitive porous plastic solids. *International Journal of Fracture* **21**, 261–278.

Pierce, D., Shih, C. F. and Needleman, A. (1984). A tangent modulus method for rate dependent solids. *Computers and Structures* **18**, 875–887.

Pijaudier-Cabot, G. and Bazant, Z. P. (1987). Nonlocal damage theory. *Journal of Engineering Mechanics ASCE* **113**, 1512–1533.

Pijaudier-Cabot, G. and Benallal, A. (1993). Strain localization and bifurcation in a nonlocal continuum. *International Journal of Solids and Structures* **30**, 1761–1775.

Puttick, D. E. (1959). Ductile fracture in metals. *Philosophy Magazine* **4**, 964–969.

Rogers, H. C. (1960). The tensile fracture of ductile metals. *Transactions of the Mettallurgical Society AIME* **218**, 498.

Sun, D.-Z. and Hönig, A. (1994). Significance of the characteristic length for micromechanical modelling of ductile fracture. In *Localized Damage III. Computer-Aided Assessment and Control* (Edited by M. H. Aliabadi *et al.*). Computational Mechanics Publications, Boston, pp. 287–296.

Tvergaard, V. (1981). Influence of voids on shear band instabilities under plane strain conditions. *International Journal of Fracture* **17**, 389–407.

Tvergaard, V. (1982). On localization in ductile materials containing spherical voids. *International Journal of Fracture* **18**, 237–252.

Tvergaard, V. (1989). Numerical study of localization in a void-sheet. *International Journal of Solids and Structures* **10**, 1143–1156.

Tvergaard, V. (1990). Material failure by void growth to coalescence. *Advances in Applied Mechanics* **27**, 83–151.

Tvergaard, V. (1996). Effect of void size difference on growth and cavitation instabilities. *Journal of Mechanics, Physics and Solids* (to appear).

Tvergaard, V. and Needleman, A. (1984). Analysis of the cup-cone fracture in a round tensile bar. *Acta Metallurgica* **32**, 157–169.

Tvergaard, V. and Needleman, A. (1992). Effect of crack meandering on dynamic, ductile fracture. *Journal of Mechanics, Physics and Solids* **40**, 447–471.

Tvergaard, V. and Needleman, A. (1995a). Effects of nonlocal damage in porous plastic solids. *International Journal of Solids and Structures* **32**, 1063–1077.

Tvergaard, V. and Needleman, A. (1995b). Nonlocal effects in ductile fracture by cavitation between larger voids. In *Computational Plasticity, Fundamentals and Applications* (Edited by D. R. J. Owen and E. Onate), pp. 963–973.